

RESEARCH ARTICLE | OCTOBER 03 2023

Characteristics of cellular structure of detonation waves propagating in annular channels

Kepeng Yao (姚克鹏) ; Pengfei Yang (杨鹏飞) ; Chun Wang (王春)  ; Zonglin Jiang (姜宗林) 



Physics of Fluids 35, 106104 (2023)

<https://doi.org/10.1063/5.0160349>



Physics of Fluids

Special Topic: K. R. Sreenivasan:
A Tribute on the occasion of his 75th Birthday

[Submit Today](#)



Characteristics of cellular structure of detonation waves propagating in annular channels

Cite as: Phys. Fluids **35**, 106104 (2023); doi: [10.1063/5.0160349](https://doi.org/10.1063/5.0160349)

Submitted: 31 May 2023 · Accepted: 11 September 2023 ·

Published Online: 3 October 2023



View Online



Export Citation



CrossMark

Kepeng Yao (姚克鹏),^{1,2}  Pengfei Yang (杨鹏飞),¹  Chun Wang (王春),^{1,2,a)}  and Zonglin Jiang (姜宗林)^{1,2} 

AFFILIATIONS

¹State Key Laboratory of High Temperature Gas Dynamics, Institute of Mechanics, Chinese Academy of Sciences, Beijing 100190, China

²School of Engineering Sciences, University of Chinese Academy of Sciences, Beijing 100049, China

^{a)} Author to whom correspondence should be addressed: wangchun@imech.ac.cn

ABSTRACT

This study investigates the characteristics of stable and unstable cells and wavefronts of detonation waves propagating in annular channels with different inner radii and channel widths using two-dimensional Euler equations along with a two-step induction-exothermic reaction kinetics. The results reveal that the effect of annular channels on the detonation cell structure depends on both the inner radius and channel width. To quantify this effect, a parameter σ is introduced, representing the ratio of the inner and outer radii of the channel. We have discovered that for values of the parameter σ exceeding a critical value σ_s , the detonation wavefront demonstrates characteristics similar to those observed in a straight channel scenario. On the contrary, when σ is below σ_s , the wavefront becomes distorted, potentially leading to Mach reflection as σ decreases further to another critical value σ_m . Additionally, the interaction among expansion waves induced by the inner walls leads to an augmented induced length and the potential occurrence of localized decoupling of the detonation wave, particularly for unstable detonation waves. However, it is worth noting that the re-initiation of the detonation wave may be triggered by the formation of hotspots resulting from the interaction between transverse shock waves and the detonation wave. This study aims to characterize the propagation characteristics of detonation waves within annular channels, with the objective of providing valuable insights for the design and optimization of annular chamber configurations in systems involving detonation.

Published under an exclusive license by AIP Publishing. <https://doi.org/10.1063/5.0160349>

I. INTRODUCTION

Detonation is an extreme combustion phenomenon that offers several advantages, such as supersonic propagation, self-initiation, rapid release of energy, and high thermal efficiency.¹ It has been widely investigated as an ideal combustion mode in hypersonic engines such as pulse detonation engines (PDEs),² oblique detonation engines (ODEs),^{3–7} and rotating detonation engines (RDEs).^{8–12} In the design of RDEs, annular combustion chambers are widely used.^{13–17} However, the geometric configuration can seriously affect the detonation propagation in the annular channel,^{18,19} even quenching the detonation. Additionally, the cellular structure formed by the interlaced loci of triple-wave points generated by the interaction of transverse shock waves and detonation plays a vital role in the stable propagation of detonation waves.^{20,21}

Cell size is one of the most fundamental dynamic parameters of combustible mixtures, strongly influenced by their physical properties.^{22–26} Higher levels of active energy lead to larger cell sizes and gradually irregular cellular structures.²³ The expansion waves induce a longer reaction zone and lead to a larger cell size of detonation waves

when the detonation wave is propagating in an expanding channel.²⁷

The Mach reflection of detonation on the wedge is observed, and its strength is sensitive to the porous media on the wedge surface.²⁸ While self-adjusting to accommodate changes in channel width, cells must adhere to the half-cell law.²⁹ Compression and expansion waves can significantly deform cells when the detonation-channel cross-section contracts, expands, or bends.³⁰ The presence of an inhomogeneous gas ahead of the detonation wave can cause a reduction in the detonation velocity, ultimately leading to the formation of a dual cellular structure involving a substructure and a larger-scale structure.³¹ Furthermore, Xi *et al.* demonstrated that the cellular morphology is determined by the ratio of longitudinal disturbance wavelength to reaction zone width.³² The inhomogeneous gas may impede detonation propagation or even quench it. However, the re-initiation of detonation can take place when the inert layer thickness is less than a critical value, through coupling with the transverse shock waves.^{33,34}

The aforementioned studies have highlighted the crucial role of transverse shock waves in ensuring the stable propagation of cellular

detonation waves. The geometry of detonation channels can impact both the generation and disappearance of transverse shock waves during detonation propagation in bent channels.^{35,36} These transverse shock waves strengthen the detonation propagation and contribute to the re-initiation of local decoupled detonations.³⁷ When curved channels are involved, compression has the primary effect on detonation waves, with the normalized radius of the channel determining the extent of this effect.³⁸ In a series of experiments, Nakayama *et al.* and Pan *et al.* found that the critical transition condition for the shift from unstable to stable mode of detonation propagation is when the inner radius of annular channels surpasses 21–32 times the detonation cellular width.^{18,39}

Detonation propagating in bend channels has been extensively studied; however, previous studies mostly focused on the propagation mode of detonation waves, with limited investigation into the characteristics of cells and wavefronts. This paper aims to address this gap by examining the fine structure of detonation waves and investigating how the coupled effects of inner radius and channel width of annular channels impact stable and unstable detonation. Furthermore, we anticipate that this study will offer valuable insights into the design and optimization of annular chamber configurations in systems that utilize detonation, such as rotating detonation engines. Additionally, it aims to enhance our understanding of detonation wave propagation within confined spaces.

II. PHYSICAL MODE AND MATHEMATIC METHODS

In this work, we first simulate the cellular detonation wave propagating in straight channels with different widths and ensure sufficient development of the detonation cells before propagating into annular channels. To initiate the detonation, a rectangular initiation zone with high pressure ($100P_0$) and high temperature ($50T_0$) is set on the near left side of the straight channel. An artificial disturbance is set in the initiation zone to accelerate the evolution of instability, which reduce computation cost. The channel walls are modeled with a slip boundary condition. All cases ensure a uniform distribution of combustible gas in the channels. The variables R and L represent the inner radius and channel width of the annular channel, respectively. The width of the straight pre-detonation channel is equal to the width of the annular channel. The schematic of the detonation wave propagating in the annular channel is shown in Fig. 1.

The detonation fields are simulated by solving the two-dimensional Euler equations together with a two-step induction-exothermic kinetic model.^{34,40,41} In this two-step reaction mechanism, the reaction variables ζ and λ represent the indices for the induction and exothermic reactions, respectively. The transport equations for the reaction variables are as follows:

$$\frac{\partial \rho \zeta}{\partial t} + \frac{\partial \rho \zeta u_j}{\partial x_j} = \omega_\zeta, \quad (1)$$

$$\frac{\partial \rho \lambda}{\partial t} + \frac{\partial \rho \lambda u_j}{\partial x_j} = \omega_\lambda, \quad (2)$$

the reaction rate computed by the Arrhenius formula

$$\omega_\zeta = H(1 - \zeta) \rho k_I \exp \left[\frac{E_I}{R} \left(\frac{1}{T_s} - \frac{1}{T} \right) \right], \quad (3)$$

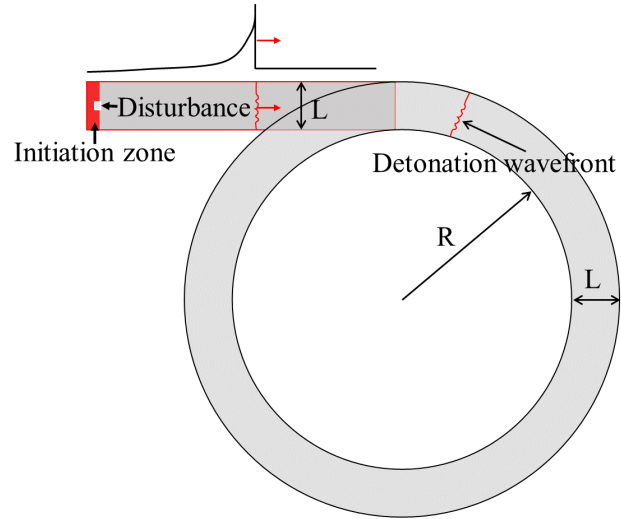


FIG. 1. The schematic of the computational model.

$$\omega_\lambda = [1 - H(1 - \zeta)] \rho (1 - \lambda) k_R \exp \left(\frac{-E_R}{RT} \right), \quad (4)$$

where E_I and E_R are the activation energies of the induction and exothermic reactions, respectively. The other variables shown here include the Heaviside step function, H , given by

$$H(1 - \zeta) = \begin{cases} 1, & \zeta < 1 \\ 0, & \zeta \geq 1, \end{cases} \quad (5)$$

as well as

$$p = \rho RT, \quad (6)$$

and

$$e = \frac{RT}{\gamma - 1} + \frac{u_j u_j}{2} + (1 - \lambda) Q, \quad (7)$$

where the variables ρ , u_j , e , T , p , γ , R , and Q are density, velocity in the j direction, specific total energy, temperature, pressure, ratio of specific heat, gas constant, and total chemical energy available in the mixture, respectively. All the variables are dimensionalized by the reference to uniform unburn state as follows:

$$\rho = \frac{\bar{\rho}}{\rho_0}, \quad p = \frac{\bar{p}}{p_0}, \quad T = \frac{\bar{T}}{T_0}, \quad u_j = \frac{\bar{u}_j}{\sqrt{R_0 T_0}}, \quad R = \frac{\bar{R}}{R_0}, \quad (8)$$

where the variables with subscript “0” are unburn state parameters, and with superscript “-” are local variables of flow field. The parameters k_I and k_R are the pre-exponential factors for the induction and exothermic reactions, respectively. In this work, $k_I = -U_{VN}$, where U_{VN} is the post shock particle velocity in the shock fixed frame for the corresponding Chapman–Jouguet (C–J) detonation, with the induction length of the C–J detonation having a fixed value of unity. In this paper, some chemical parameters are constant: $E_R = 0.7$, $k_R = 1.5$.

The governing equations were discretized on Cartesian grids. The Weighted Essentially Non-Oscillatory (WENO) schemes⁴² together with the flux vector splitting method proposed by Steger and Warming⁴³ were adopted to solve these equations. The third-order Runge–Kutta algorithm has been selected as the time-discretization scheme to facilitate high-resolution simulations. The mean grid width is 0.1, which corresponds to ten grid units over the induction length of the C–J detonation. This grid size is sufficient for the purposes of this study.³⁴ Furthermore, all the analyzed detonation fields in this study were simulated using our reliable in-house code, which has undergone extensive verification in previous studies.^{41,44}

III. RESULTS AND DISCUSSION

A. Basic structure of cellular detonation propagating in straight channel

In this subsection, we examine the propagation of detonation waves in straight channels with varying widths. Two distinct modes of detonation can be observed, characterized by their wavefronts and cellular structures. The first mode is stable and exhibits a regular cellular structure, while the second mode is unstable and displays an irregular cellular structure due to the splitting and merging of cells during its evolution. These two modes of detonation are accurately simulated using our proprietary in-house code. The simulations are performed with two sets of chemical reaction parameters derived from a detailed reaction mechanism of hydrogen and oxygen under different operating conditions. The stable parameters are $q=7.0$, $E_1=4.0$, and $\gamma=1.309$; the unstable parameters are $q=10.761$, $E_1=6.2$, and $\gamma=1.313$.

In the case of stable detonation, the wavefront appears relatively regular, albeit distorted by transverse shock waves. Two neighboring transverse shock waves travel in opposite directions, resulting in a periodic wavefront structure that can be observed laterally, as shown in Fig. 2. The high temperature and pressure behind the Mach stem, which is formed by the interaction of the traveling transverse shock wave with the detonation wavefront, lead to closely coupled chemical reactions. The results also show that there is a non-linear relationship between the tube width and the number of transverse shock waves. Specifically, in channels with lengths of 60, 120, and 240, the number of transverse shock waves observed was 5, 10, and 21, respectively.

Figure 3 depicts a lateral view of the maximum pressure histories in exquisite detail for stable detonation propagating in channels of varying widths. The channels with lengths of 60, 120, and 240 have 2.5, 5, and 10.5 cells laterally, respectively. The cellular structure of the detonation waves is highly regular, with identical cell sizes in both longitudinal and lateral directions, respectively. However, the cell width varies due to self-adjustment in channels of different widths.²⁹ The highest pressure occurs at the vertex of each cellular cell, and these pressure values are almost equal.

To analyze the characteristics of unstable detonation waves propagating in different-width straight channels, we examine the temperature contours shown in Fig. 4. Compared to stable detonation, unstable detonation exhibits fewer transverse shock waves over the evolution of cellular detonation in identical-width channels. The irregular wavefront is characterized by an inhomogeneous distribution of transverse shock waves, resulting in unreacted pockets behind the detonation wave. Additionally, neighboring transverse shock waves may travel in opposite or identical directions, which is unlike stable

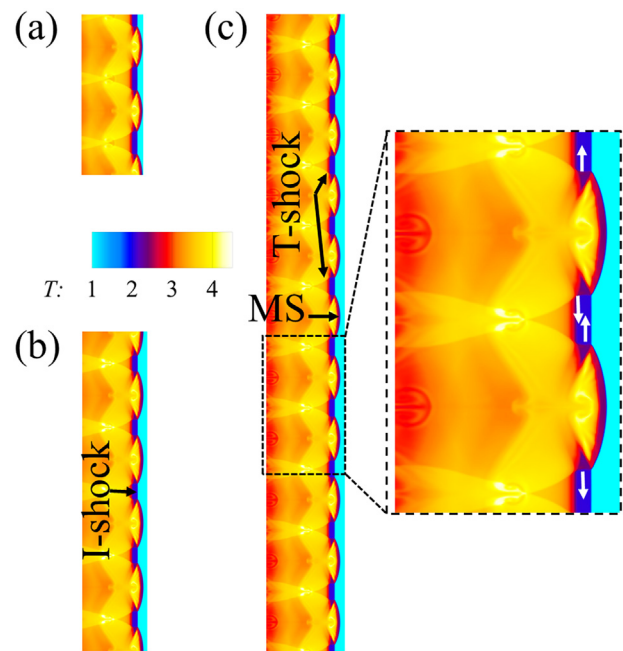


FIG. 2. Temperature contours of stable detonation propagating in different-width straight channels: (a) $L=60$, (b) $L=120$, and (c) $L=240$. T-shock: transverse shock wave, I-shock: incident shock wave, MS: Mach stem, white arrow: moving direction of transverse shock waves.

detonation. As a result, the wavefront becomes more distorted and loses its periodic characteristic.

Figure 5 presents the lateral views of maximum pressure histories for unstable detonations propagating in channels of varying widths. In contrast to stable detonation, the cellular structure of unstable detonation is irregular, and the detonation cell size varies during the

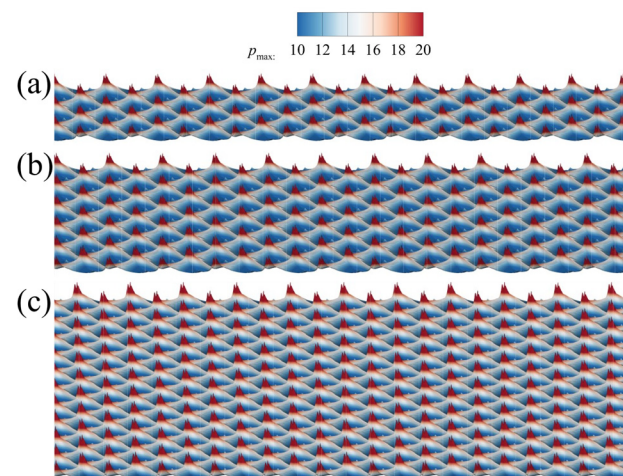


FIG. 3. Cellular structures of stable detonation propagating in different-width straight channels: (a) $L=60$, (b) $L=120$, and (c) $L=240$. White arrow: moving direction of transverse shock waves.

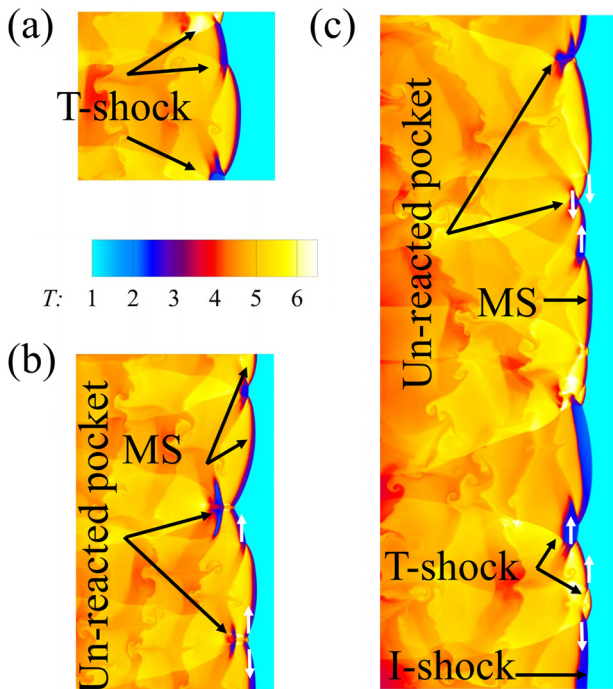


FIG. 4. Temperature contours of unstable detonation propagating in different-width straight channels: (a) $L = 60$, (b) $L = 120$, and (c) $L = 240$.

evolution of detonation. Additionally, the splitting and merging of cells are observed during unstable detonation wave propagation. The new transverse shock waves emerge as a result of the evolution of detonation wavefront fold, the new triple-wave point locus causes the detonation cell to divide into two distinct cells. Conversely, when a transverse

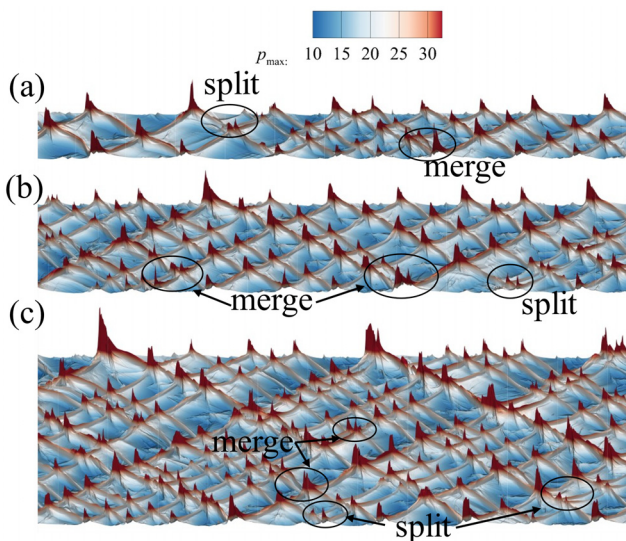


FIG. 5. Cellular structures of unstable detonation propagating in different-width straight channels: (a) $L = 60$, (b) $L = 120$, and (c) $L = 240$.

shock wave dissipates as it moving toward a region with the high thermodynamic parameters, it results in the loss of a triple-wave point locus. Consequently, this leads to the convergence and merging of the two detonation cells, resulting in a single unified cell. Similar to stable detonation, the highest pressure occurs at the vertex of each cell. However, the pressure values differ from vertex to vertex.

B. Cellular structure of stable detonation propagating in annular channel

This subsection focuses on stable detonation propagating in annular channels with uniform combustible gas. The detonation develops sufficiently in a straight channel with an identical width before propagating into the annular channel. Once the detonation wave enters the annular channel, the straight channel is swiftly removed from the system. Additionally, we have explicitly confirmed that the detonation wave within the annular channel propagates and rotates continuously without any interruptions. However, this study aims to evaluate the effect of the inner radius and width of the annular channel on the cellular structure and wavefront of the detonation wave. We only illustrate the cellular structure of detonation propagation in the annular channel during its first loop.

Figure 6 illustrates the cellular structure of detonation propagation in one cycle in annular channels with different inner radii. As the detonation propagates into the annular channel, the cells become deformed due to interaction of compression waves induced by the outer wall and expansion waves induced by the inner wall. The detonation self-adaptively adjusts the cells by generating or quenching transverse shock waves. For example, in the annular channel with $L = 60$, when the inner radius is $R = 720$ and 480 , there are 2.5 regular cells laterally in the channel, which is identical to the straight channel. However, reducing the inner radius to $R = 240$ reduces the regularity of the cellular structure, and the splitting and merging of cells are observed. When decreasing the inner radius further to $R = 120$, the cellular structure becomes even more irregular, with the pressure near the inner wall being much less than that near the outer wall, as shown in Fig. 6(a).

For the annular channel with $L = 120$, the cellular structure is regular and similar to that of the straight channel when $R = 720$. However, the number of cells is 4.5, which is less than that in the straight channel. The splitting and merging of cells are observed near the upper wall, and the split cells are very small. However, when the inner radius is decreased to $R = 480$, the cellular structure becomes deformed, with the cells compressed near the outer wall. When the inner radius is further decreased to $R = 240$, the cells near the outer wall are compressed even more, while those near the inner wall expand. With an inner radius of $R = 120$, more transverse shock waves are observed near the outer wall than the inner wall, leading to the quenching and re-initiation of the detonation wave near the lower wall, as shown in Fig. 6(b).

In the scenario with $L = 240$, there is a high-pressure zone near the upper wall, where the cells are compressed by the outer wall. The length of the high-pressure zone decreases with the decrease in the inner radius R , and the cellular structure deforms due to the generation and evanishment of transverse shock waves. Particularly for the scenario with $R = 120$, there are no obviously fish-scale cells when the detonation develops sufficiently in the annular channel. The effect of

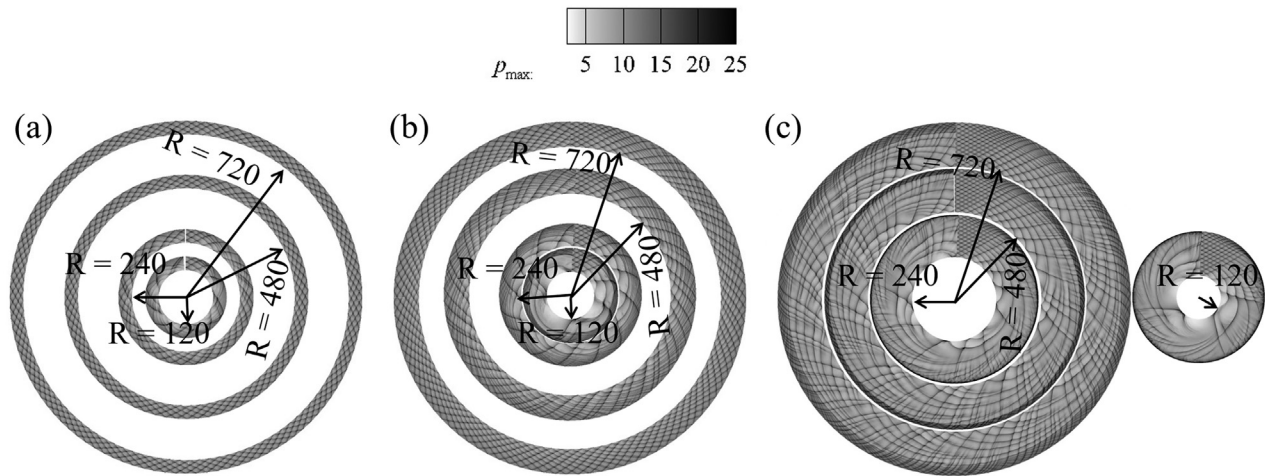


FIG. 6. Cellular structures of stable detonation propagating in annular channel with different R and L : (a) $L = 60$, (b) $L = 120$, and (c) $L = 240$.

the annular channel on the cellular structure decreases with an increase in the inner radius R .

To further examine how the annular channel deforms the cells, we will analyze the evolution of the detonation wavefront. Figure 7 displays the wavefronts of cellular detonation propagating in the annular channel with $L = 60$. It is evident that the wavefronts of detonation are almost identical when propagating in annular channels with $R = 720$ and 480, and there are five transverse shock waves, which is identical to the scenario with the straight channel, as shown in Figs. 7(a) and 7(b). However, for the scenario with $R = 240$, the detonation

propagation accompanies with the decoupling and re-initiation of the wavefront. This phenomenon arises from the reduction in the inner radius of the annular channel, which reinforces the expansion effect caused by the inner wall. This results in an augmented induced length and the potential occurrence of localized decoupling of the detonation wave. The interaction between the transverse shock wave and the detonation wave gives rise to a Mach stem with enhanced compression capability, ultimately triggering the re-initiation of the detonation wave. When the inner radius is decreased to $R = 120$, the decoupled region becomes larger, and there are transverse shock waves generated

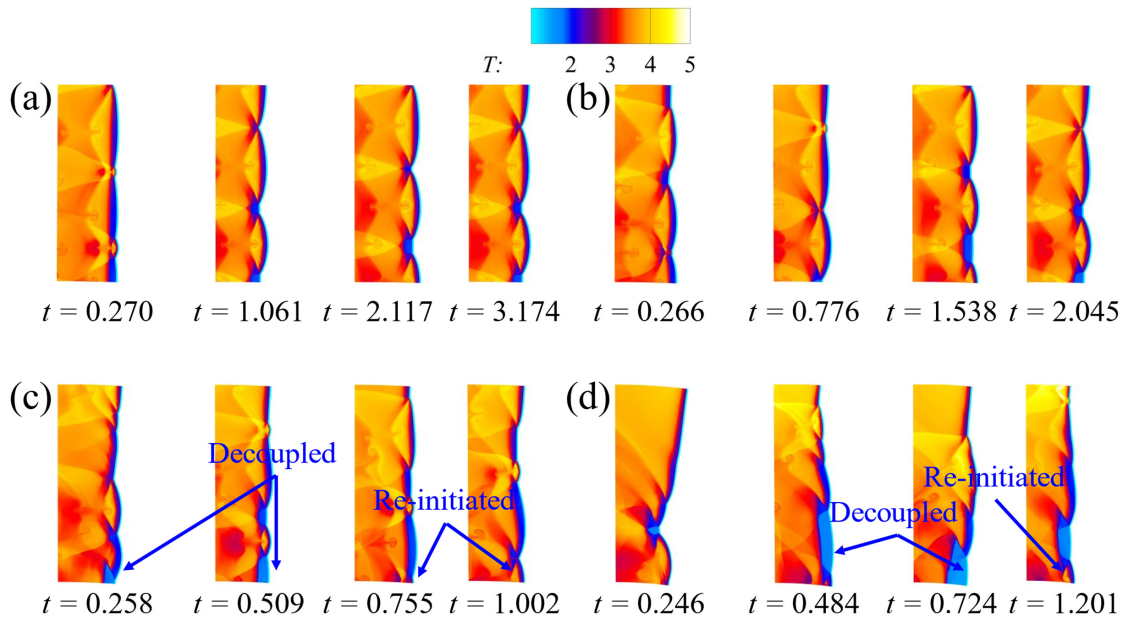


FIG. 7. Temperature contours of stable detonation propagating in the annular channel with $L = 60$: (a) $R = 720$, (b) $R = 480$, (c) $R = 240$, and (d) $R = 120$.

and vanished as they are compressed and expanded by the annular channel walls. Thus, it can be concluded that the annular channel with a smaller inner radius has a greater impact on the cellular structure and wavefront of the detonation.

For the scenario with $L = 120$, the detonation does not exhibit decoupled behavior when the inner radius is $R = 720$. However, at the early stage of detonation propagating into the annular channel ($t = 0.252$), there are some neighboring transverse shock waves traveling in the same direction, indicating the generation of new transverse shock waves. Afterward, the distribution of transverse shock waves becomes similar to that in the straight channel due to the self-adaptive adjustment of the detonation wave, as shown in Fig. 8(a). In the case with $R = 480$, more pairs of neighboring transverse shock waves with the same traveling direction are observed throughout the propagation of detonation wave, as shown in Fig. 8(b). With further decrease in the inner radius to $R = 240$, the number of left-traveling transverse shock waves is much less than that of the right-traveling waves. In this case, the detonation wave decouples and re-initiates near the lower wall, as shown in Fig. 8(c). Figure 8(d) shows the wavefront of the scenario with $R = 120$, where the decoupled region is larger and there is a Mach stem with many transverse shock waves generated by the interaction between the detonation wave and the upper wall. The length of Mach stem changes with the evolution of detonation waves.

Figure 9 illustrates the wavefronts of cellular detonation propagating in the annular channel with $L = 240$. As the inner radius R decreases from 720 to 480, the detonation wave interacts with the upper wall and forms a Mach stem with multiple transverse shock waves, as demonstrated in Figs. 9(a) and 9(b). Further decreasing the inner radius to $R = 240$ also results in the formation of a Mach stem, but with a shorter length compare to those with larger inner radii. Additionally, the detonation wave decouples and re-initiates locally near the inner wall, as observed in Fig. 9(c). Based on these results, it can be inferred that the length of the Mach stem decreases with a

decrease in the inner radius of the annular channel. In Fig. 9(d), the wavefront shows no Mach stem when $R = 120$. However, a reflected transverse shock wave is formed due to the interaction of the detonation wave with the upper wall, and the decoupled region near the lower wall is larger than that of the case with $R = 240$.

In summary, the subsection investigates the effect of the inner radius of an annular channel on stable detonation propagation in a varying width channel. The cellular structure and wavefronts of cellular detonations are shown for different inner radii of the annular channel. It is observed that the annular channel with a smaller inner radius has a more significant effect on the detonation propagation, as it leads to decoupled and re-initiated wavefronts, the formation and disappearance of transverse shock wave.

C. Cellular structure of unstable detonation propagating in annular channel

This subsection presents an analysis of the cellular structures exhibited by unstable detonation waves propagating in annular channels with varying inner radii and widths. Figure 10 illustrates the different cellular structures observed in annular channels with varying inner radii and lengths. For channels with a width of 60, the cellular structures in channels with inner radii of 720 and 480 are comparable to those observed in straight channels. However, upon decreasing the inner radius to 240 and 120, a series of discontinuous low-pressure regions near the inner wall are observed, indicative of the quenching and re-initiation of the detonation wave, as shown in Fig. 10(a). For channels with a width of 120, the detonations do not continuously decouple when the inner radius is set to 720 and 480. Additionally, the average size of the cells is smaller than that those observed in straight channels. However, upon decreasing the inner radius to 240, a region of no-transverse shock waves and high-pressure zones is observed near the inner wall, indicating the decoupling and re-initiation of the

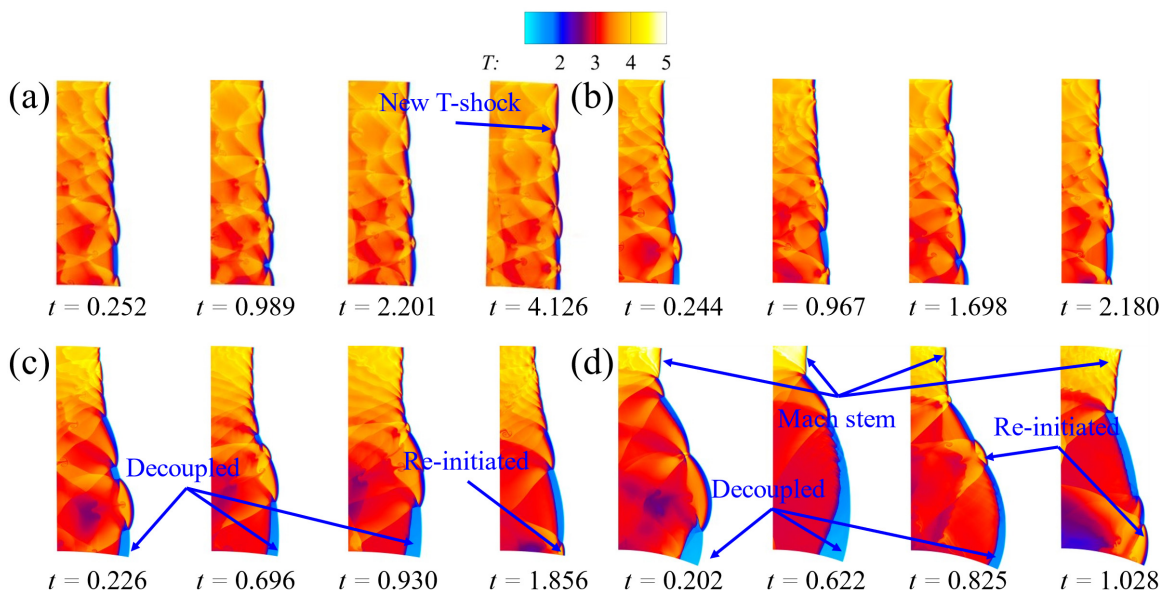


FIG. 8. Temperature contours of stable detonation propagating in the annular channel with $L = 120$: (a) $R = 720$, (b) $R = 480$, (c) $R = 240$, and (d) $R = 120$.

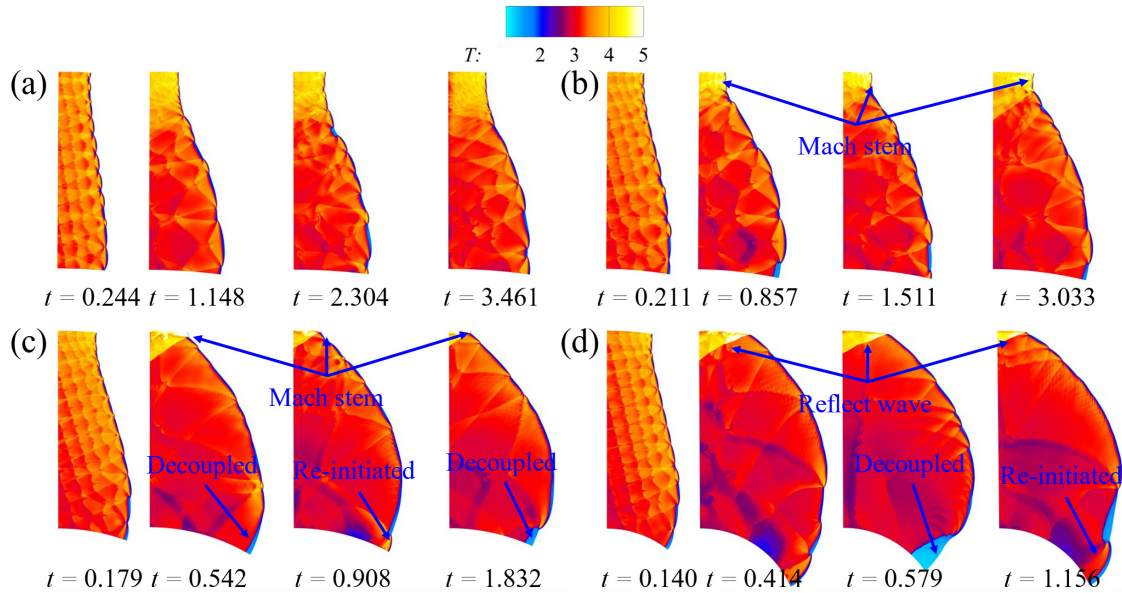


FIG. 9. Temperature contours of stable detonation propagating in the annular channel with $L = 240$: (a) $R = 720$, (b) $R = 480$, (c) $R = 240$, and (d) $R = 120$.

detonation wave in this region. When further decreasing the inner radius to $R = 120$, the detonation wave is observed to decouple noticeably near the inner wall, as shown in Fig. 10(b). Figure 10(c) presents the cellular structure of the scenario with a length of 240. It can be observed that the detonation wave decouples and re-initiates near the inner wall, with the size of the decoupled region increasing with decreasing inner radius.

Here, we discuss the wavefront characteristics of unstable detonation propagating in an annular channel with $L = 60$, as presented in Fig. 11. In comparison with the stable detonation described earlier, the unstable detonation displays a more deformed wavefront with unreacted

pockets behind the detonation wave. As depicted in Figs. 11(a) and 11(b), the detonation may locally decouple near the outer wall, in contrast to the stable detonation that only decouples near the inner wall. The reason for this is that the reaction surface is primarily coupled with the Mach stem on the wavefront. Additionally, the expansion waves induced by the inner wall reduce the number of transverse shock waves, resulting in a smaller Mach stem region on the wavefront. As a result, decoupling of the detonation occurs near the outer wall for the unstable detonation waves. However, the decoupled region is re-initiated by the transverse shock wave. When decreasing the inner radius to $R = 240$ and 120 , the decoupled zone becomes larger

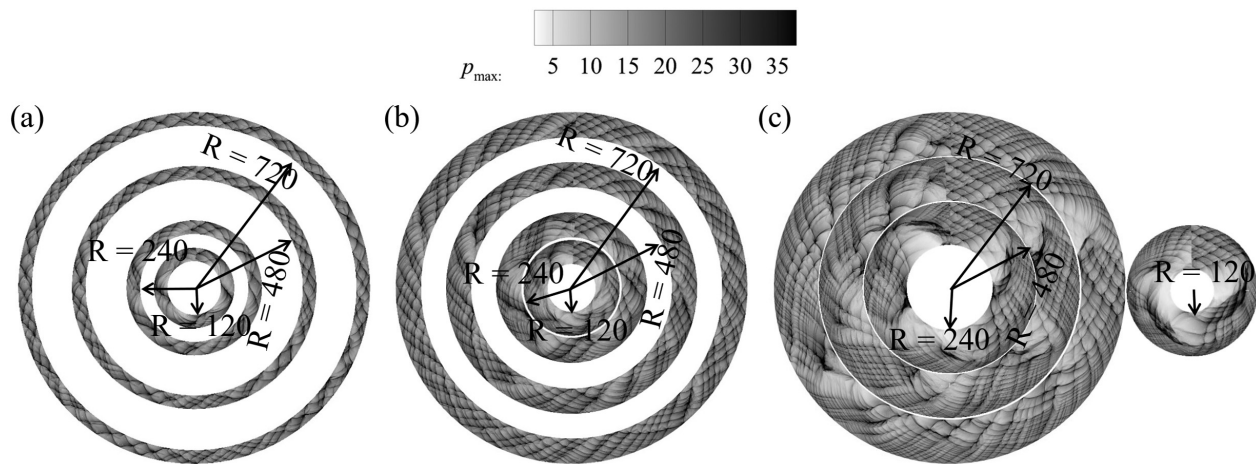


FIG. 10. Cellular structures of unstable detonation propagating in annular channel with different R and L : (a) $L = 60$, (b) $L = 120$, and (c) $L = 240$.

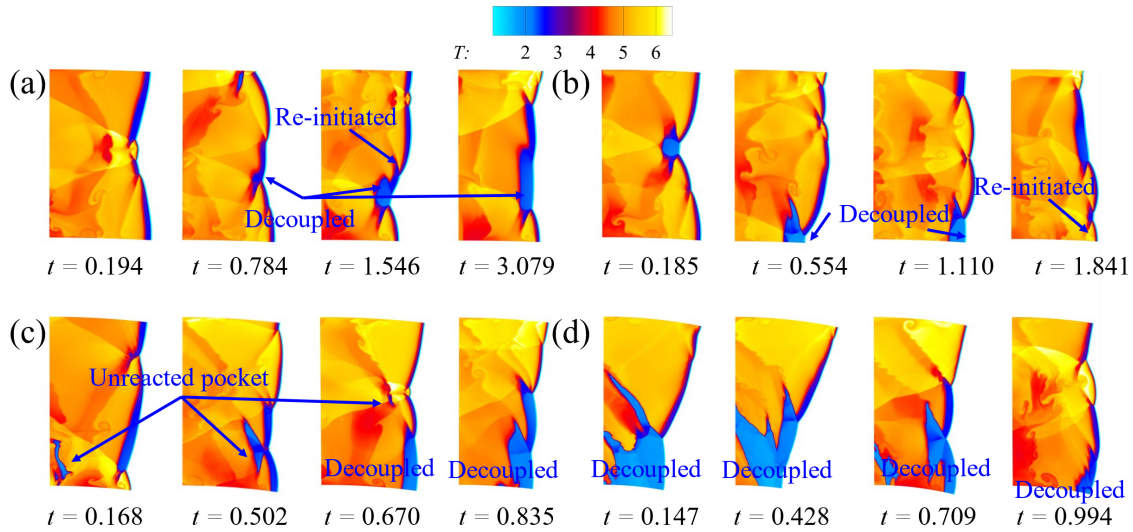


FIG. 11. Temperature contours of unstable detonation propagating in the annular channel with $L = 60$: (a) $R = 720$, (b) $R = 480$, (c) $R = 240$, and (d) $R = 120$.

and more prominent near the inner wall. This behavior can be attributed to the increased strength of the expansion and compression waves generated by the inner and outer walls with a decrease in the inner radius, as shown in Figs. 11(c) and 11(d).

In the scenario where $L = 120$, the detonation wave is observed to decouple and re-initiate near the inner wall, with the decoupled region increasing in size as the inner radius decreases, as depicted in Fig. 12. The phenomenon of decoupling only occurs near the inner wall for inner radii of $R = 240$ and 120 , with a larger number of transverse shock waves moving from top to bottom, as shown in Figs. 12(c) and 12(d). A similar trend is observed in the scenario where $L = 240$, with a larger decoupled zone. Furthermore, in the top-half of the wavefront, there are a greater number of transverse shock waves than

in the other half, with most of the transverse shock waves traveling from top to bottom, as depicted in Fig. 13. Notably, for inner radii of $R = 240$ and 120 , normal detonation waves are re-initiated by the transverse shock wave in the larger decoupled region, as shown in Figs. 13(c) and 13(d). These observations provide valuable insights into the behavior of unstable detonation waves propagating in annular channels with varying geometries.

D. Effects of annular channel on the detonation cells

The above results indicate that the annular channel has a significant impact on both cellular structure and wavefront of detonation. The influence of annular channel increases with an increasing channel

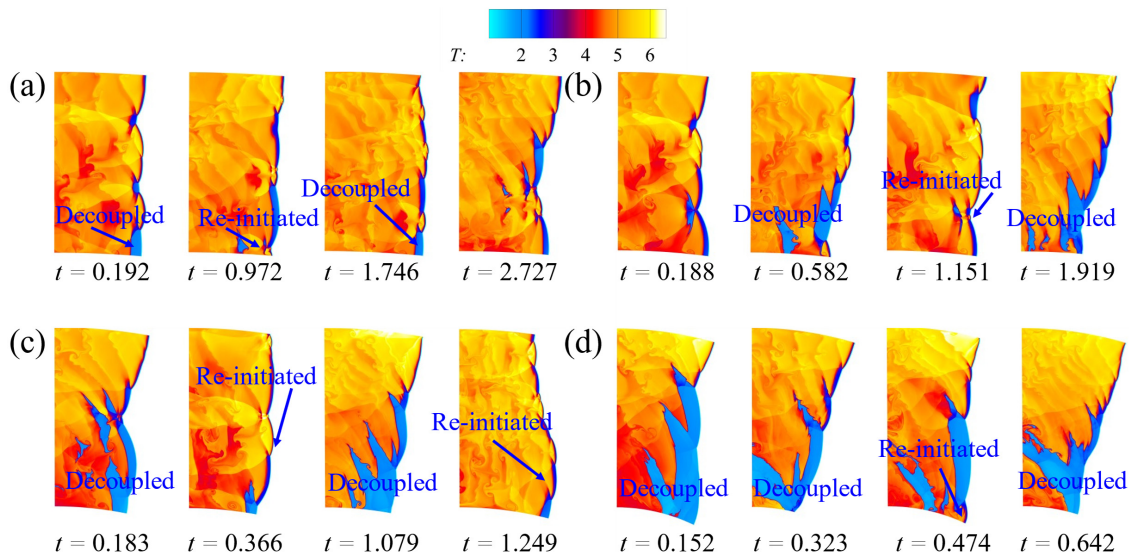


FIG. 12. Temperature contours of unstable detonation propagating in the annular channel with $L = 120$: (a) $R = 720$, (b) $R = 480$, (c) $R = 240$, and (d) $R = 120$.

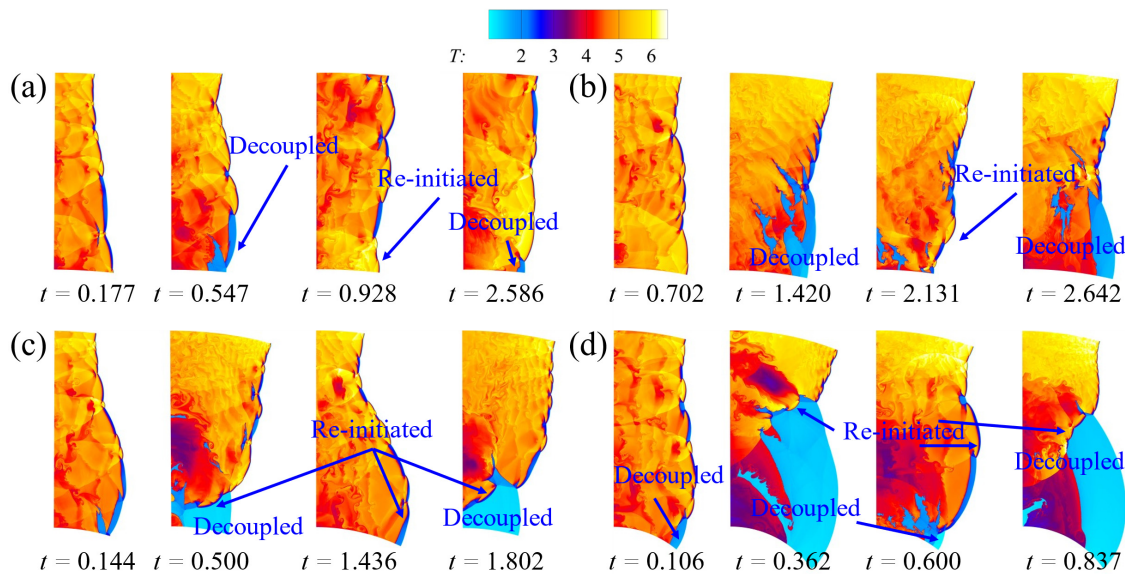


FIG. 13. Temperature contours of unstable detonation propagating in the annular channel with $L = 240$: (a) $R = 720$, (b) $R = 480$, (c) $R = 240$, and (d) $R = 120$.

width for a specific inner radius and decreases with a reduced inner radius for a specific channel width. Furthermore, when the inner radius of the annular channel reaches a critical value, the cellular structure becomes identical to that of straight channels. To further demonstrate this phenomenon, additional simulations were conducted and their results are illustrated in Fig. 14. The critical radius was found to

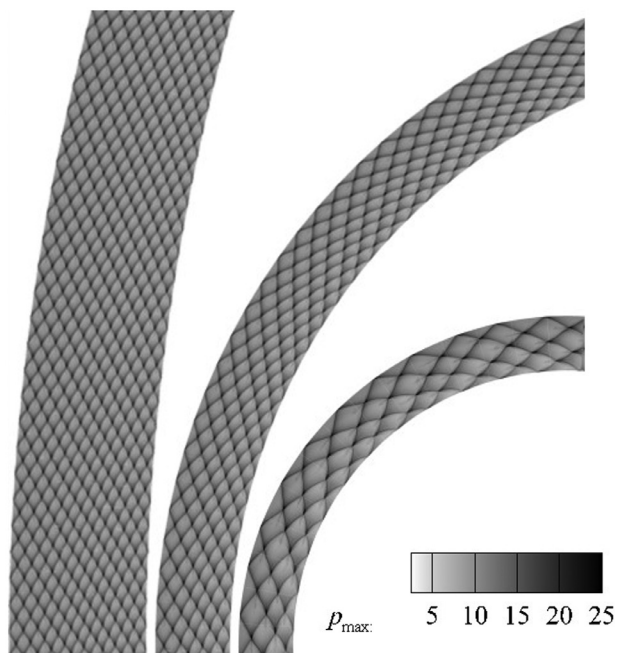


FIG. 14. Cellular structure in annular channel for different channel width is identical to straight channel.

be 300, 960, and 4060 for scenarios with $L = 60$, 120, and 240 respectively.

Based on the above descriptions, Mach/regular reflection takes place on the near outer walls when the inner radius of the annular channels decreases to another critical value. Therefore, the detonation wave propagating in the annular channels can be distinguished into four modes: (a) Has an identical cellular structure to the detonation propagating in the straight channel; (b) the number of cells is less than the straight channel scenario, and the cellular structure gradually transitions to irregular; (c) the cells deform more noticeably, and Mach reflection structure are formed by the interaction of detonation and outer wall; and (d) the regular reflection structure is formed by the interaction of detonation wave and out wall. The schematic of these modes of detonation is shown in Fig. 15.

Based on the above description, both the inner radius and width of annular channel affect the modes of detonation. In order to further investigate how the annular channel configuration affects the detonation waves, we introduce the ratio of inner and outer radius (σ) to reflect the effects of the annular channel. More cases are conducted to analyze the effect of annular channel configuration on the modes of detonation waves quantitatively, and that is indicated in Fig. 16. The existence of two critical values, σ_s and σ_m , plays a decisive role in determining the modes of detonation. In scenarios where the ratio of the inner and outer radius exceeds σ_s , the detonation cell structure remains unchanged and resembles that of a straight channel. However, as the ratio of the inner and outer radius decreases below σ_s , the detonation cells undergo deformation, and the transition to irregular shapes occurs. Further reduction in this ratio, falling below σ_m , results in the formation of a Mach stem due to the interaction between the detonation and the outer wall. Both critical values exhibit an increasing trend as the channel width, denoted by L , increases. However, the observation of the regular reflection mode is confined solely to the scenario wherein $L = 240$, thereby confirming that this mode exclusively manifests in scenarios characterized by a wider width

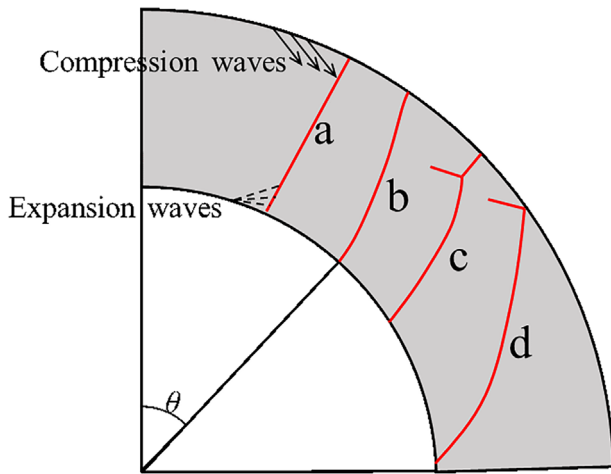


FIG. 15. The schematic of four modes of detonation propagating in the annular channel.

and a smaller inner radius. The findings from this analysis hold practical implications for RDE. Understanding the effects of the inner radius and channel width on detonation modes can assist in designing and optimizing annular channel configurations in systems involving detonation waves.

To further explore the effect of the annular channel on the cellular structure of detonation, we extracted the pressure history along the inner and outer walls of stable detonation propagation in an annular channel with $L = 240$, as shown in Fig. 17. Here, the variable θ represents the angle at which the detonation wave propagates in the annular channel. In the early stages of detonation propagation into the annular channel, there is a self-adaptive adjustment stage (Stage I), characterized by a gradual increase in detonation pressure along the upper wall and corresponding decrease along the lower wall. This stage becomes more prominent as the inner radius decreases. The pressure along the outer wall exhibits a relatively stable state, with a higher minimum and oscillation frequency compared to the inner wall. As the inner radius decreases, the pressure peak along the outer wall increases while the peak along the inner wall decreases. This is attributed to the increased strength of compression and expansion waves with a smaller inner

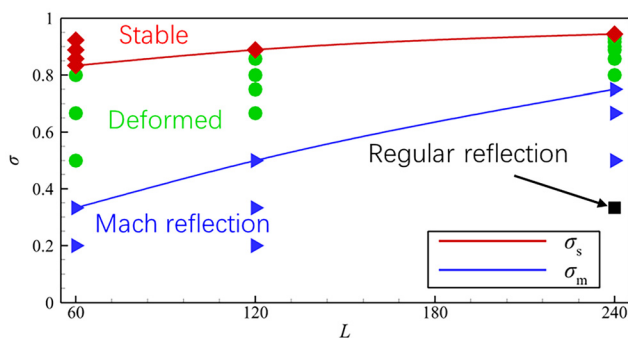


FIG. 16. Critical condition of different modes of detonation.

radius. The difference in pressure between the outer and inner wall also increases as the inner radius decreases, indicating a reduction in the difference of velocity between the two walls.

Figure 18 shows the maximum pressure along the outer and inner wall of stable detonation propagating in an annular channel with different values of R and L . By comparing Figs. 17(b) and 17(d), it can be observed that both the self-adaptive adjustment stage and the pressure peak along the outer wall decrease with decreasing channel width. Furthermore, the detonation has a regular pressure oscillation and the oscillation frequency of pressure along the outer and inner wall is almost equal when the channel configuration is $R = 480$ and $L = 60$, as shown in Fig. 18(b). It can be concluded that the effect of annular channel on detonation propagation decreases with increasing inner radius and decreasing channel width. Upon comparing it with Fig. 17(a), it becomes apparent that the pressure disparity between the outer and inner walls escalates as the channel width L increases. This observation implies that the discrepancy in velocity between the inner and outer walls diminishes as L increases.

Based on the above description, it is evident that the detonation velocity along the outer and inner walls gradually increases and decreases, respectively, during the self-adaptive adjustment stage. The ratio of angle velocity along outer and inner wall decrease to 1 from $1/\sigma$. In this stage, the detonation wavefront gradually deforms, and the degree of deformation ultimately determines the modes of detonation propagation in the annular channels. Additionally, unstable detonation often experiences significant decoupling due to the expansion interaction induced by the inner wall, leading to a significant reduction in the angular velocity along the inner wall. This distortion of the cell structure occurs even when the value of σ is relatively high because the detonation propagation involves decoupled detonations.

IV. CONCLUSION

In this work, two-dimensional Euler equations along with the two-step induction–exothermic reaction kinetic are adopted to simulate the cellular detonation propagating in the annular channels. A pre-detonation straight channel with an identical channel-width to the annular channel is set to ensure sufficient development of cellular detonation before propagating into the annular channels. The effects of the inner radius and channel width on the cellular structure of detonation waves are investigated. The results show that the cellular structure is sensitive to the inner radius and channel width of annular channels. As the inner radius decreases, the cellular structure undergoes gradual deformation. A smaller channel width leads to a smaller deformation of the cellular structure. To quantify the effect of annular channels on the cells, we introduce a parameter σ that represents the ratio of inner and outer radius of annular channels. The influence of the annular channel on the detonation becomes significant as the parameter σ deviates further from 1.0. As σ decreases, we identify four modes of detonation wave: (a) Identical cell structure to that of a straight channel (stable mode); (b) reduced number and regularity of cells (deformed mode); (c) more obvious cell deformation and the formation of a Mach reflection structure by the interaction of detonation and outer wall (Mach reflection mode); and (d) regular reflection structure formed by the interaction of the detonation wave and outer wall (regular reflection mode). Two critical values, σ_s and σ_m , are presented to distinguish between the modes of

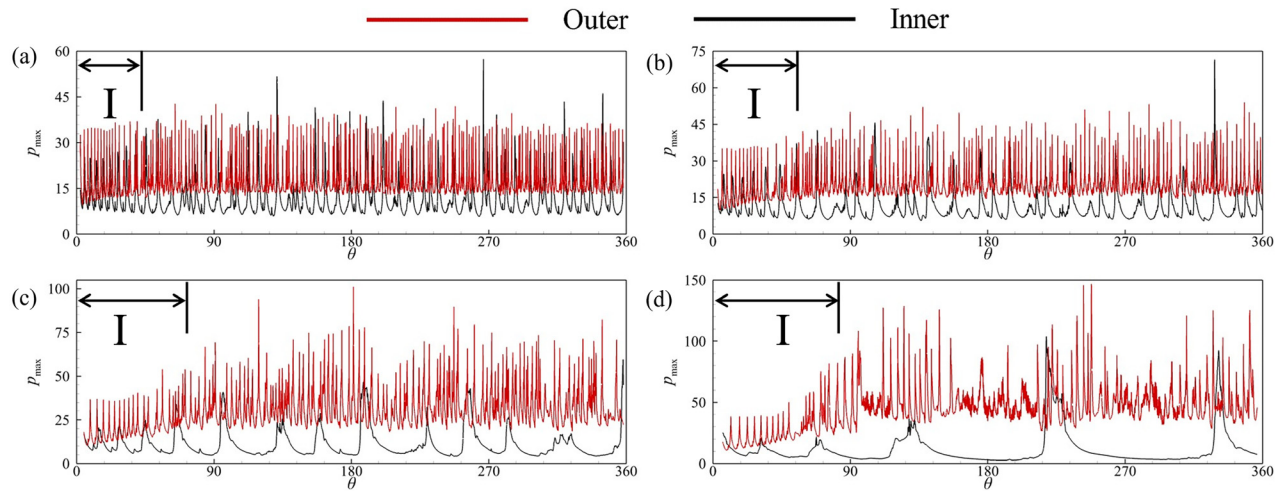


FIG. 17. The pressure maximum along upper wall and lower wall of stable detonation propagating in the annular channel with $L = 240$: (a) $R = 720$, (b) $R = 480$, (c) $R = 240$, and (d) $R = 120$.

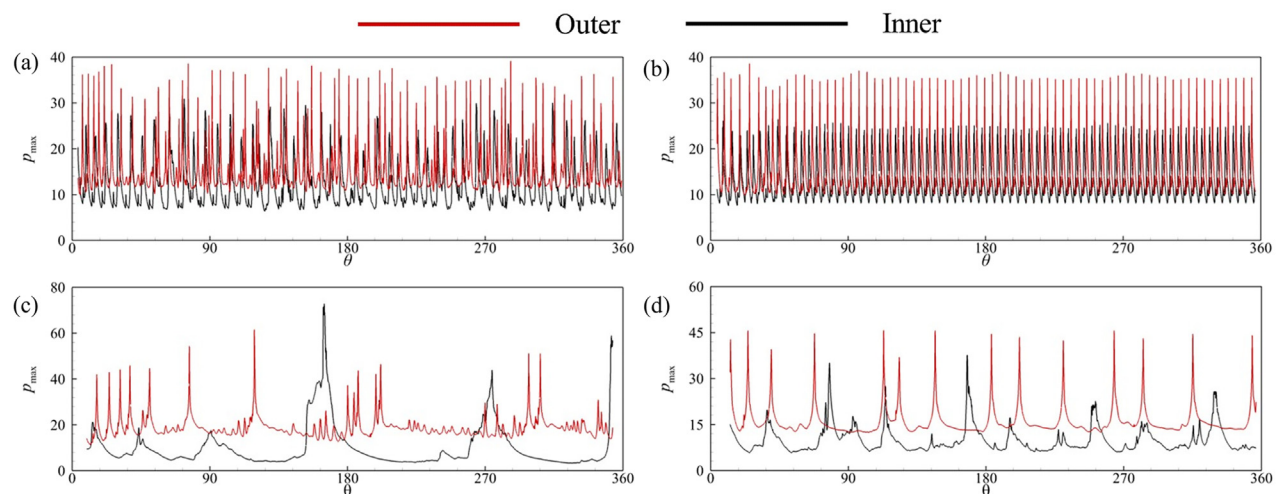


FIG. 18. The pressure maximum along upper wall and lower wall of stable detonation propagating in the annular channel with (a) $R = 480$, $L = 120$, (b) $R = 480$, $L = 60$, (c) $R = 120$, $L = 120$, and (d) $R = 120$, $L = 60$.

detonation waves propagating in annular channels. The regular reflection mode only occurs in scenarios with larger channel widths. Additionally, the expansion interaction of the inner wall also causes local decoupling of detonation waves, which reduces the detonation velocity along the inner wall and significantly distorts the cellular structure, especially for unstable detonation waves. However, the re-initiation of detonation waves occurs due to the interaction between transverse shock waves and the detonation wave, forming a hotspot that initiates the detonation waves.

ACKNOWLEDGMENTS

This work has been supported by the National Natural Science Foundation of China (Grant Nos. 12072353, 12132017, and 12202014).

AUTHOR DECLARATIONS

Conflict of Interest

The authors have no conflicts to disclose.

Author Contributions

Kepong Yao: Data curation (equal); Investigation (equal); Software (equal); Validation (equal); Writing – original draft (equal). **Pengfei Yang:** Funding acquisition (equal); Investigation (equal); Methodology (equal); Writing – original draft (equal). **Chun Wang:** Methodology (equal); Software (equal); Validation (equal); Writing – original draft (equal). **Zonglin Jiang:** Investigation (equal); Methodology (equal); Software (supporting); Validation (equal).

DATA AVAILABILITY

The data that support the findings of this study are available from the corresponding author upon reasonable request.

APPENDIX: THE VALIDATION OF COMPUTATION SOLVER AND GRID RESOLUTIONS

We would like to emphasize the rigorous analysis conducted on all the detonation fields, which were simulated using our well-established in-house code. This code has been extensively verified through prior studies, ensuring its reliability. Furthermore, we have compared the ZND structure between our CFD results and theoretical models, which clearly demonstrate a high level of agreement. This can be observed in Fig. 19, where the ZND structures are almost coincident, providing strong support for the accuracy of our simulation results. To further reinforce the credibility of our in-house code, we have conducted a comparison between the CFD-calculated CJ detonation velocity and the theoretical CJ detonation velocity. This comparison yielded an error value of less than 0.5%, affirming the excellent agreement between the calculations and the theoretical predictions.

Furthermore, we conducted an analysis of the grid resolution. Two different grid resolutions were implemented during the

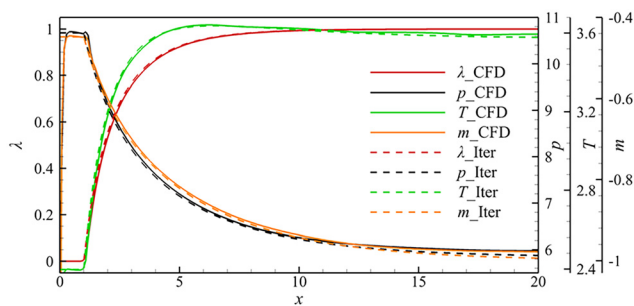


FIG. 19. The ZND structure of one-dimensional simulation and the theoretical.

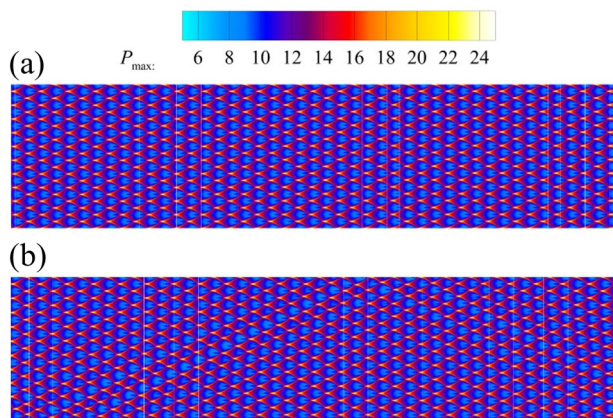


FIG. 20. The detonation cells simulated by different grid resolutions: (a) grid width is 0.1 and (b) grid width is 0.05.

numerical simulations, with dimensionless grid scales of 0.1 and 0.05, respectively. As illustrated in Fig. 20, it can be observed that the resulting mean cell sizes from these various grid resolutions are remarkably consistent. Consequently, for the purposes of this study, a grid resolution of 0.1 was deemed appropriate to simulate detonation cells, as it struck a balance between computational complexity and simulation accuracy. This decision is considered reasonable and justified.

REFERENCES

- P. Wolański, "Detonative propulsion," *Proc. Combust. Inst.* **34**, 125–158 (2013).
- F. Ma, J.-Y. Choi, and V. Yang, "Thrust chamber dynamics and propulsive performance of multitube pulse detonation engines," *J. Propul. Power* **21**, 681–691 (2005).
- Z. Jiang, Z. Zhang, Y. Liu, C. Wang, and C. Luo, "The criteria for hypersonic airbreathing propulsion and its experimental verification," *Chin. J. Aeronaut.* **34**, 94–104 (2021).
- Z. Xu, G. Dong, Z. Pan, and M. Gui, "Standing window of oblique detonation with pathological behaviour," *Chin. J. Aeronaut.* **34**, 496–503 (2021).
- L. Yang, L. Yue, D. Yu, and Z. Chen, "Numerical study on wave configuration of wedge-induced oblique detonation wave: Reactive boundary layer effect," *Phys. Fluids* **34**, 116103 (2022).
- G. Xiang, X. Gao, W. Tang, X. Jie, and X. Huang, "Numerical study on transition structures of oblique detonations with expansion wave from finite-length cowl," *Phys. Fluids* **32**, 056108 (2020).
- Y. Fang, Y. Zhang, X. Deng, and H. Teng, "Structure of wedge-induced oblique detonation in acetylene-oxygen-argon mixtures," *Phys. Fluids* **31**, 026108 (2019).
- M. Zhao, M. J. Cleary, and H. Zhang, "Combustion mode and wave multiplicity in rotating detonative combustion with separate reactant injection," *Combust. Flame* **225**, 291–304 (2021).
- K. Yao, P. Yang, H. Teng, Z. Chen, and C. Wang, "Effects of injection parameters on propagation patterns of hydrogen-fueled rotating detonation waves," *Int. J. Hydrogen Energy* **47**, 38811–38822 (2022).
- W. Zhu, Y. Wang, and J. Wang, "Flow field of a rotating detonation engine fueled by carbon," *Phys. Fluids* **34**, 073311 (2022).
- Q. Meng, N. Zhao, and H. Zhang, "On the distributions of fuel droplets and *in situ* vapor in rotating detonation combustion with prevaporized n-heptane sprays," *Phys. Fluids* **33**, 043307 (2021).
- Y. Liu, W. Zhou, Y. Yang, Z. Liu, and J. Wang, "Numerical study on the instabilities in H₂-air rotating detonation engines," *Phys. Fluids* **30**, 046106 (2018).
- R. Zhou and J. Wang, "Numerical investigation of flow particle paths and thermodynamic performance of continuously rotating detonation engines," *Combust. Flame* **159**, 3632–3645 (2012).
- Z. Pan, B. Fan, X. Zhang, M. Gui, and G. Dong, "Wavelet pattern and self-sustained mechanism of gaseous detonation rotating in a coaxial cylinder," *Combust. Flame* **158**, 2220–2228 (2011).
- C. Yan, H. Teng, and H. D. Ng, "Effects of slot injection on detonation wavelet characteristics in a rotating detonation engine," *Acta Astronaut.* **182**, 274–285 (2021).
- H. Teng, L. Zhou, P. Yang, and Z. Jiang, "Numerical investigation of wavelet features in rotating detonations with a two-step induction-reaction model," *Int. J. Hydrogen Energy* **45**, 4991–5001 (2020).
- W. Fan, S. Liu, S. Zhong, H. Peng, X. Yuan, and W. Liu, "Characteristics of ethylene-air continuous rotating detonation in the cavity-based annular combustor," *Phys. Fluids* **35**, 045142 (2023).
- Z. Pan, J. Qi, J. Pan, P. Zhang, Y. Zhu, and M. Gui, "Fabrication of a helical detonation channel: Effect of initial pressure on the detonation propagation modes of ethylene/oxygen mixtures," *Combust. Flame* **192**, 1–9 (2018).
- V. R. Katta, K. Y. Cho, J. L. Hoke, J. R. Codoni, F. R. Schauer, and W. M. Roquemore, "Effect of increasing channel width on the structure of rotating detonation wave," *Proc. Combust. Inst.* **37**, 3575–3583 (2019).
- X. Lu, C. R. Kaplan, and E. S. Oran, "A chemical-diffusive model for simulating detonative combustion with constrained detonation cell sizes," *Combust. Flame* **230**, 111417 (2021).

- ²¹W. Han, C. Wang, and C. K. Law, "Role of transversal concentration gradient in detonation propagation," *J. Fluid Mech.* **865**, 602–649 (2019).
- ²²J. H. S. Lee, "Dynamic parameters of gaseous detonations," *Annu. Rev. Fluid Mech.* **16**, 311–336 (1984).
- ²³V. N. Gamezo and D. Desbordes, "Formation and evolution of two-dimensional cellular detonations," *Combust. Flame* **116**, 154–165 (1999).
- ²⁴F. Pintgen, C. A. Eckett, J. M. Austin, and J. E. Shepherd, "Direct observations of reaction zone structure in propagating detonations," *Combust. Flame* **133**, 211–229 (2003).
- ²⁵W. Han, J. Huang, and C. Wang, "Pulsating and cellular instabilities of hydrogen–oxygen detonations with ozone sensitization," *Phys. Fluids* **33**, 076113 (2021).
- ²⁶M. Reynaud, F. Virost, and A. Chinnayya, "A computational study of the interaction of gaseous detonations with a compressible layer," *Phys. Fluids* **29**, 056101 (2017).
- ²⁷Q. Xiao and C. Weng, "Effect of losses on hydrogen–oxygen–argon detonation cell sizes," *Phys. Fluids* **33**, 116103 (2021).
- ²⁸D. Chen, H. Ma, and L. Wang, "Mach reflection of detonation wave on porous wall," *Phys. Fluids* **35**, 037109 (2023).
- ²⁹C. Wang, Z. Jiang, and Y. Gao, "Half-cell law of regular cellular detonation," *Chin. Phys. Lett.* **25**, 3704–3707 (2008).
- ³⁰G. O. Thomas and R. L. Williams, "Detonation interaction with wedges and bends," *Shock Waves* **11**, 481–492 (2002).
- ³¹Y. Wang, C. Huang, R. Deiterding, H. Chen, and Z. Chen, "Numerical studies on detonation propagation in inhomogeneous mixtures with periodic reactant concentration gradient," *J. Fluid Mech.* **955**, A23 (2023).
- ³²X. Xi, H. Teng, Z. Chen, and P. Yang, "Effects of longitudinal disturbances on two-dimensional detonation waves," *Phys. Rev. Fluid* **7**, 043201 (2022).
- ³³Y. Wang, J. Su, R. Deiterding, and Z. Chen, "Effects of dilution and pressure on detonation propagation across an inert layer," *AIAA J.* **61**, 1540 (2023).
- ³⁴H. Li, W. Han, J. Li, and W. Fan, "Influences of incoming flow on re-initiation of cellular detonations," *Combust. Flame* **229**, 111376 (2021).
- ³⁵D. Zhang, X. Yuan, S. Liu, X. Cai, H. Peng, R. Deiterding, and H. D. Ng, "Numerical study of detonation wave propagation modes in annular channels," *AIP Adv.* **11**, 085203 (2021).
- ³⁶X. Yuan, J. Zhou, X. Mi, and H. D. Ng, "Numerical study of cellular detonation wave reflection over a cylindrical concave wedge," *Combust. Flame* **202**, 179–194 (2019).
- ³⁷M. Peswani and B. Maxwell, "Detonation wave diffraction in stoichiometric C_2H_4/O_2 mixtures using a global four-step combustion model," *Phys. Fluids* **34**, 106104 (2022).
- ³⁸S. H. Lee, D. R. Jo, and J. Y. Choi, "Effect of curvature on the detonation wave propagation characteristics in annular channels," AIAA Paper No. 2008-988, 2008.
- ³⁹H. Nakayama, T. Moriya, J. Kasahara, A. Matsuo, Y. Sasamoto, and I. Funaki, "Stable detonation wave propagation in rectangular-cross-section curved channels," *Combust. Flame* **159**, 859–869 (2012).
- ⁴⁰H. D. Ng, M. I. Radulescu, A. J. Higgins, N. Nikiforakis, and J. H. S. Lee, "Numerical investigation of the instability for one-dimensional Chapman–Jouguet detonations with chain-branching kinetics," *Combust. Theory Model* **9**, 385–401 (2005).
- ⁴¹P. Yang, H. Li, Z. Chen, C. Wang, and H. Teng, "Numerical investigation on movement of triple points on oblique detonation surfaces," *Phys. Fluids* **34**, 066113 (2022).
- ⁴²G. S. Jiang and C. W. Shu, "Efficient implementation of weighted ENO schemes," *J. Comput. Phys.* **126**, 202–228 (1996).
- ⁴³J. L. Steger and R. F. Warming, "Flux vector splitting of the inviscid gas-dynamic equations with application to finite-difference methods," *J. Comput. Phys.* **40**, 263–293 (1981).
- ⁴⁴K. Yao, P. Yang, H. Li, C. Wang, and Z. Jiang, "Characteristics of reattached oblique detonation induced by a double wedge," *Phys. Fluids* **35**, 036112 (2023).